AMSE JOURNALS –2015-Series: Modelling B; Vol. 84; N° 2; pp 52-79
Submitted Aug. 2015; Revised Oct. 30, 2015; Accepted Nov. 30, 2015

Steady Free Convection Heat and Mass Transfer MHD Flow of a Radiative Micropolar Fluid in a Vertical Porous Channel with Heat Source and Chemical Reaction

M. K. Nayak

Department of Physics, Radhakrishna Institute of Technology and Engineering,
Biju Patnaik University of Technology, Odisha, India (E-mail: mnkec1973@gmail.com)

Abstract

In this paper a steady free convection heat and mass transfer flow of a radiative conducting micropolar fluid in a vertical porous channel in the presence of temperature dependent heat source/sink, chemical reaction and thermal radiation under the influence of a transverse magnetic field is investigated. The numerical solutions of the governing differential equations are obtained by fourth order Runge-Kutta method and are presented for a wide range of emerging parameters. A striking result is to note that microrotation is independent of the material property and vortex viscocity in the middle layers of the channel. The resistive force offered by the porous matrix affects the motion of the flow so as to decelarate the velocity in both symmetric and asymmetric cases. It is inferred that an increase in radiation parameter enhances the heat transfer which in turn produces a significant increase in the thickness of thermal boundary layer.

Key words: Free convection, Micropolar fluid, Chemical reaction, Magnetic field, Porous channel, Thermal radiation.

1. Introduction

Micropolar fluids proposed by Eringen [1] simulate accurately the flow characteristics of polymeric additives, geomorphological sediments, colloidal and haematological suspensions, liquid crystals, lubricants etc. Nayak [2] has presented many ideas about synthesis and characteristic properties of several micropolar fluids related to industrial applications. The flows of heat convection in micropolar fluids past on flat surfaces was studied by Rahman et al. [3-7].

The problem of fully developed natural convection heat and mass transfer of a micropolar fluid between porous vertical plates with asymmetric wall temperatures and concentrations is analyzed by Abdulaziz and Hashim [8]. Later, El-Arabawy [9] has shown the effect of suction/injection on the flow of a micropolar fluid past a continuously moving plate in the presence of radiation. Nayak et al. [10] observed the natural convection MHD flow of a viscoelastic fluid through an inclined porous plate. The numerical and analytical solutions of the developing laminar free convection of a micropolar fluid in vertical parallel plate channel involving asymmetric heating are analyzed by Chamkha et al. [11].

Nomenclature

B	material parameter	C_p	specific heat at constant pressure
C	non-dimensional species concentration	C_0	reference species concentration
D	diffusion coefficient	E	total heat rate added to the fluid
g	acceleration due to gravity	H_0	uniform transverse magnetic field
j	micro-inertial density	k	kinematic rotational viscosity
K_c	chemical reaction parameter	L	distance between two vertical walls
m	temperature ratio parameter	M	magnetic parameter
m_1	concentration ratio parameter	K_p	permeability parameter
Q	volume flow rate	R	vortex viscosity parameter
S	heat source/sink parameter	t	non-dimensional time
T	non-dimensional temperature	T_0	reference temperature
u	non-dimensional velocity	ω	micro-rotation velocity
K_p	permeability parameter		

Greek letters

α	thermal diffusivity	λ	radiation parameter
γ	local buoyancy parameter	μ	dynamic viscosity
ρ	density of the fluid		

MHD heat and mass transfer in a rotating system with periodic suction was studied by Parida et al. [12]. Recently, Zueco et al. [13] studied magneto-micropolar fluid over a stretching surface embedded in a Darcian porous medium by the numerical network method. Further, Eldabe et al. [14] reported their work on hydromagnetic peristaltic flow on micropolar biviscocity fluid. Another interesting work related to MHD visco-elastic flow with heat and mass transfer was reported very recently by Kar et al. [15].

The porous matrix is included because the flow and heat transport processes occur by using insulating material (porous matrix) that greatly prevents heat loss/energy loss and accelerates the process of cooling/heating as the case may be serving as a heat exchanger. Helmy et al. [16] studied MHD free convection flow of a micropolar fluid past a vertical porous plate. Also the effect of chemical reaction on MHD flow of a viscoelastic fluid through porous medium was studied by Nayak et al. [17]. Mohanty et al. [18] investigated numerically the heat and mass transfer effect of micropolar fluid over a stretching sheet through porous media. Many researchers like [19-23] studied the effect of porosity on micropolar fluid flow.

Flow of fluids with internal heat sources/sinks are of great practical as well as theoretical interest. The fluid motion develops slowly due to the development of non-uniformity in the temperature field. The volumetric heat generation/absorption term exerts strong influence on the flow and heat transfer with appreciably large temperature difference. The analysis of temperature field as modified by the heat source / sink in moving fluid is important in view of chemical reaction and problem concerned with dissociating fluids. Foraboschi et al. [24] have assumed two state volumetric heat generation depending on temperature difference as

$$\theta = \begin{cases} \theta_0 (T - T_0), & T \geq T_0 \\ 0, & T < T_0 \end{cases}$$

Thermal radiation factor is better suitable for cooling process. The effect of radiation and viscous dissipation on stagnation-point flow of a micropolar fluid over a nonlinearly stretching surface with suction/injection was discussed by Babu et al. [25].

In many chemical engineering processes chemical reaction occurs between a foreign mass and the working fluid which moves due to stretching or otherwise of a surface. The effect of chemical reaction on a moving isothermal vertical surface with suction was studied by Muthucumaraswamy [26].

Very recently, Nayak et al. [27] have made an investigation on the steady free convection and mass transfer MHD flow of a micropolar fluid in a vertical channel with heat source and chemical reaction. However, they have not studied the effect of porous matrix and thermal radiation in their study.

The purpose of the present study is to establish a mathematical model of a conducting radiative micropolar fluid flow, heat and mass transfer in a vertical porous channel under the influence of porous matrix as well as transverse magnetic field. The heat transfer associated with internal temperature dependent volumetric heat source/sink as well as concentration distribution accompanied by the chemical reaction of the reactive species obeying a first order reaction subject to a resistive force offered by porous matrix in presence of thermal radiation is the main theme of the modeling. One of the important aspects in this study is the investigation of the effects of porosity and thermal radiation over and above other physical parameters on the velocity and microrotation. The numerical solutions are obtained and analyzed to bring out the effects of various emerging parameters.

The relevance of present investigation lies in geothermal areas where flow of chemically treated ground water or industrial fluid showing micropolar fluid properties occurs. Moreover, installation of porous matrix and application of transverse magnetic field fixed to the body contribute to slow down the heat transfer at the stagnation point and enhances the body's drag. Both these outcomes are desirable for protecting a vehicle reentering the atmosphere as studied by Cramer and Pai [28].

2. Mathematical formulation

Consider a steady laminar free convective MHD flow of a radiative conducting micropolar fluid between two vertical porous walls subjected to a transversely applied magnetic field where the induced electric current due to the motion of the fluid does not distort the applied magnetic field. This assumption is true if the magnetic Reynolds number of the flow is very small as in the case of many aerodynamic applications involving low velocities and electrical conductivities.

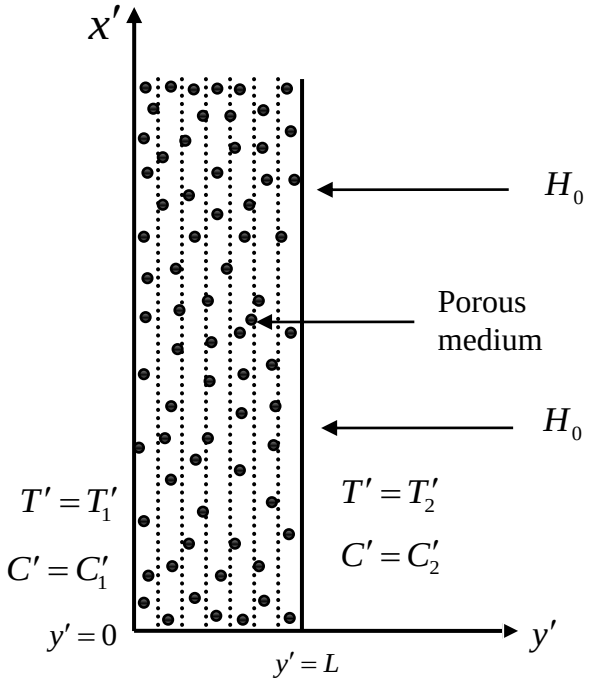

Fig. 1: Schematic diagram of the flow model.

The vertical porous walls are separated by a distance L and having temperatures T_1' and T_2' and concentrations C_1' and C_2' . The $x'-$ axis is taken along one of the vertical walls while $y'-$ axis is normal to it [Fig.1]. The walls are assumed to be infinitely long so that the dependent variables are independent of the vertical co-ordinate. For free convection, let us consider a vertical channel with walls maintained at different temperatures and concentrations in still micropolar fluid. The velocity of the fluid due to free convection heat and mass transfer within the plates is small. Hence, the dissipation due to viscosity is neglected in this problem but body forces due to gravity are included following Pai [29]. The micropolar fluid may be considered as an incompressible fluid if the temperature and concentration gradients are not appreciably large. Under these assumptions the governing equations corresponding to the established model can be obtained as :

$$(\mu + k)\frac{d^2u'}{dy'^2} + k\frac{d\omega'}{dy'} + \rho g\frac{T' - T_0'}{T_0'} + \rho g\frac{C' - C_0'}{C_0'} - \sigma H_0^2 u' - \frac{\mu u'}{K_p'} = 0 \quad (1)$$

$$\gamma\frac{d^2\omega'}{dy'^2} - k(2\omega' + \frac{du'}{dy'}) = 0 \quad (2)$$

$$\alpha\frac{d^2T'}{dy'^2} + S'(T' - T_0') - \frac{1}{\rho Cp}\frac{dq_r}{dy'} = 0 \quad (3)$$

$$D\frac{d^2C'}{dy'^2}+K_c'(C'-C_0')=0 \tag{4}$$

where $\gamma=(\mu+0.5k)\,j$, $\alpha=\dfrac{k}{\rho C_p}$

The boundary conditions are

$$\left.\begin{aligned} u'=0,\omega'=-\frac{1}{2}\frac{du'}{dy'},T'=T_1',C'=C_1' \quad at\ y'=0\\ u'=0,\omega'=-\frac{1}{2}\frac{du'}{dy'},T'=T_2',C'=C_2' \quad at\ y'=L \end{aligned}\right\} \tag{5}$$

In the energy equation the heat due to viscous dissipation is neglected for small velocities due to free convection heat and mass transfer with the plates. Soret-Dufour (thermal diffusion and diffusion-thermo) effects are also ignored in the diffusion equations which is true when the species concentration level is very low.

By using Rosseland approximation for thermal radiation [30] the radiative heat flux is modeled as

$$q_r=-\frac{4\sigma_1}{3k_1}\frac{\partial(T'^4)}{\partial y'}$$

where σ_1 is the Stefan-Boltzmann constant and k_1 is the mean absorption coefficient.

We assume that the differences in temperature within the flow are such that the non-linear term T'^4 can be expressed as a linear combination of the temperature. This is obtained by expanding T'^4 in a Taylor series about T_∞ and neglecting higher order terms [31], we obtain

$$T'^4 \cong 4T_\infty^3T'-3T_\infty^4$$

and thus the gradient of heat radiation term can be expressed as

$$\frac{\partial q_r}{\partial y'}=-\frac{16\sigma_1T_\infty^3}{3k_1}\frac{\partial^2T'}{\partial y'^2}$$

Using the above expression, eqn. (3) the takes the form

$$\alpha\frac{d^2T'}{dy'^2}+S'(T'-T_0')+\frac{16\sigma_1T_\infty^3}{3k_1\rho Cp}\frac{dq_r}{dy'}=0 \tag{6}$$

Introducing the following non-dimensional quantities,

$$\left.\begin{aligned} &y = y'/L,\ \omega = \frac{\omega'\mu}{\rho g\, L}, u = \frac{u'\mu}{\rho g L^2}, M^2 = \frac{\sigma H_0^2 L^2}{\mu}, \\ &T = \frac{T' - T_0'}{T_0'}, C = \frac{C' - C_0'}{C_0'}, m = \frac{T_2' - T_0'}{T_0'}, m_1 = \frac{C_2' - C_0'}{C_0'} \\ &B = L^2/j, S = S'L^2/\alpha, K_c = K_c' L^2/D, K_p = \frac{K_p'}{L^2}, R = k/\mu, K_p = \frac{L^2}{K_p'}, \lambda = \frac{16\sigma_1 T_\infty^3}{3kk_1} \end{aligned}\right\} \quad (7)$$

the equations (1), (2), (6) and (4) take the form

$$(1+R)\frac{d^2u}{dy^2} + R\frac{d\omega}{dy} - \left(M^2 + K_p\right)u = -T - C \quad (8)$$

$$\left(1+\frac{R}{2}\right)\frac{d^2\omega}{dy^2} - BR\left(2\omega + \frac{du}{dy}\right) = 0 \quad (9)$$

$$\frac{d^2T}{dy^2} + (S+\lambda)T = 0 \quad (10)$$

$$\frac{d^2C}{dy^2} + K_c C = 0 \quad (11)$$

and the corresponding boundary conditions (5) become

$$\left.\begin{aligned} &u = 0, \omega = -\frac{1}{2}\frac{du}{dy}, T = 1, C = 1 \quad at\ y = 0 \\ &u = 0, \omega = -\frac{1}{2}\frac{du}{dy}, T = m, C = m_1 \quad at\ y = 1 \end{aligned}\right\} \quad (12)$$

3. Numerical solution

The governing equations are solved numerically by employing fourth order Runge-Kutta method along with shooting technique. This method provides accurate results for boundary layer equations. In the present calculations, the value of *y* is considered as 1 and grid size or step size of *y* is considered as $\Delta y = 0.001$ and the convergence criterion is set to 10^{-5} for better consideration of boundary conditions. The solutions are achieved for the dimensionless velocity, microrotation, temperature and concentration and shown graphically.

Let $u = y_1, u' = y_2, \omega = y_3,\ \omega' = y_4, T = y_5,\ T' = y_6,\ C = y_7$ and $C' = y_8$.

so that $y_2' = \frac{1}{1+R}\left[\left(M^2 + K_p\right)y_1 - R\,y_4 - y_5 - y_7\right]$,

$$y'_4 = \frac{1}{1+R/2}\left[BR\left(2y_3 + y_2\right)\right],$$

$$y'_6 = -(S+\lambda)y_5$$

and $$y'_8 = -K_c y_7$$

with $y_a(1)=0$, $y_b(1)=0$, $y_a(3)=-0.5y_a(2)$, $y_b(3)=-0.5y_b(2)$, $y_a(5)=1$, $y_b(5)=m$, $y_a(7)=1$ and $y_b(7)=m_1$.

4. Results and discussion

The boundary layer governing equations for the problem of heat and mass transfer effects of a steady free convective MHD flow of a radiative micropolar fluid between two vertical porous walls in the presence of heat source/sink and chemical reaction are solved numerically by fourth order Runge-Kutta method along with shooting technique. The solutions are represented for different values of several governing parameters and the results are presented through graphs and tables.

It is inevitable to know the effects of mass transfer, heat transfer, chemical reaction parameter, permeability parameter and thermal radiation parameter of the reacting species on the flow field. For the purpose of calculation we have assumed two cases (i) under symmetric distribution of temperature and concentration ($m = m_1 = 1$) i.e., $T'_2 = 2T'_0$ and $C'_2 = 2C'_0$ which correspond to the temperature and concentration at the plate $y = 1$ are twice the reference temperature and concentration. Moreover, $T = 1$ and $C = 1$, boundary conditions, correspond to $T_1' = 2T_0'$ and $C_1' = 2C_0'$. Hence, the results lead to the case of equal temperature and concentration (ii) asymmetric distribution ($m = m_1 = 0$) corresponds to unequal temperature and concentration at the plates.

The parabolic velocity distribution indicates a common characteristic i.e. presence of heat source and exothermic reaction **(**$S > 0, K_c > 0$**)** escalating the velocity at all points in comparison with the case of sink and endothermic reaction $(S < 0, K_c < 0)$ overrides the effects of other pertinent parameters on the flow phenomena for both symmetric and asymmetric temperature and concentration distribution.

The velocity distribution is almost symmetrical about the middle of the channel involving a crest at $y = 0.5$ (approx.).

Moreover, from equations (8) and (9), it is clear that vortex viscosity parameter *R* attributes micropolar property, even enjoys more priority than material parameter *B*. If *R* =0 both the governing equations reduce to

$$\frac{d^2u}{dy^2} = -T - C,$$

$$\frac{d^2\omega}{dy^2} = 0$$

which infer that effect of material parameter automatically becomes ineffective.

Fig. 2 (asymmetric case : $m = m_1 = 0$) portrays the velocity distribution for different values of *R*, *S*, *B* and K_c for both source and exothermic reaction $(S > 0, K_c > 0)$ as well as sink and endothermic reaction $(S < 0, K_c < 0)$. It is observed that an increase in *S* and K_c enhances velocity whereas increase in *R*, decreases it in the presence of source and exothermic reaction as well as sink and endothermic reaction. But there is a fall in velocity due to increase in *B* in the source and exothermic reaction whereas opposite effect is observed due to sink and endothermic reaction. Fig. 3 (symmetric case : $m = m_1 = 1$) displays the velocity profiles with different values of *R*, *S*, *B* and K_c for both $S > 0, K_c > 0$ and $S < 0, K_c < 0$. The effects of all the parameters qualitatively remain same as that of asymmetric case besides symmetricity of the distribution.

From Figs. 4 and 5, it is noticed that the effect of Lorentz force due to the interaction of magnetic field with conducting micropolar fluid opposes the motion of the flow as a result of which the value of the velocity decreases in both $m = m_1 = 0$ and $m = m_1 = 1$.

Figs. 6 and 7 represent the velocity profiles for asymmetric and symmetric distribution of temperature and concentration. It is interesting to note that the profiles are not affected due to change in material parameter in the absence of heat source and chemical reaction, however, the velocity is decelerated substantially due to the vortex viscosity $R\left(=\frac{k}{\mu}\right)$. Thus, it is obvious that kinematic rotational viscosity resists the flow causing a thinner hydrodynamic boundary layer.

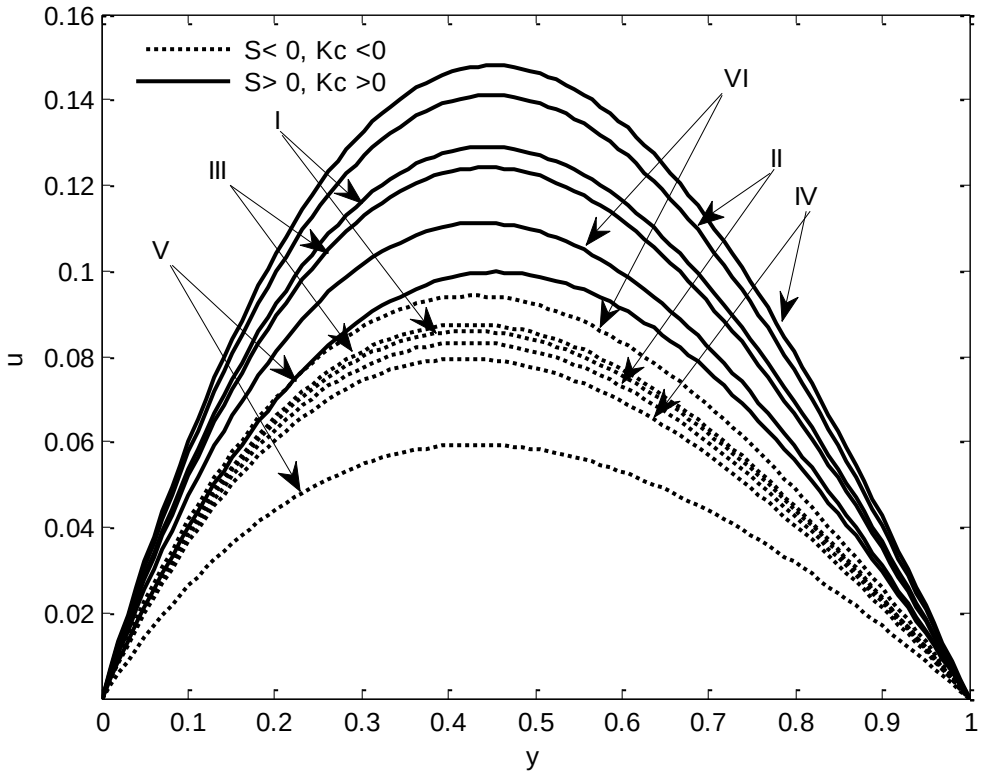

Curve	R	S	B	Kc	Curve	R	S	B	Kc
I	0.5	1.0	0.5	3.0	I	0.5	-1.0	0.5	-3.0
II	0.5	1.0	0.5	4.0	II	0.5	-1.0	0.5	-4.0
III	0.5	1.0	1.0	4.0	III	0.5	-1.0	1.0	-4.0
IV	0.5	2.0	0.5	4.0	IV	0.5	-2.0	0.5	-4.0
V	1.5	1.0	0.5	4.0	V	1.5	-1.0	0.5	-4.0
VI	0.5	1.0	0.5	0.7	VI	0.5	-1.0	0.5	-0.7

Fig 2 : Velocity profiles showing effects of R, S, B , K_c **for** $M = K_p = \lambda = 0$ **and** $m = m_1 = 0$.

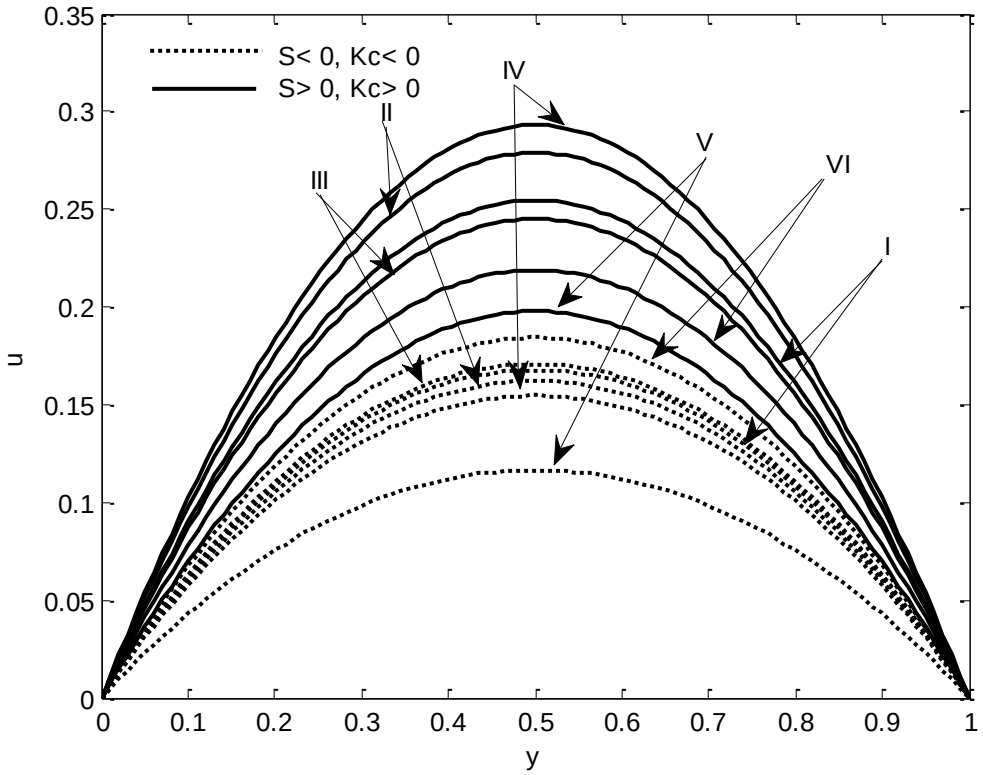

Curve	R	S	B	Kc	Curve	R	S	B	Kc
I	0.5	1.0	0.5	3.0	I	0.5	-1.0	0.5	-3.0
II	0.5	1.0	0.5	4.0	II	0.5	-1.0	0.5	-4.0
III	0.5	1.0	1.0	4.0	III	0.5	-1.0	1.0	-4.0
IV	0.5	2.0	0.5	4.0	IV	0.5	-2.0	0.5	-4.0
V	1.5	1.0	0.5	4.0	V	1.5	-1.0	0.5	-4.0
VI	0.5	1.0	0.5	0.7	VI	0.5	-1.0	0.5	-0.7

Fig 3: Velocity profiles showing the effects of R, S, B, K_c **for** $M = K_p = \lambda = 0$ **and** $m = m_1 = 1$.

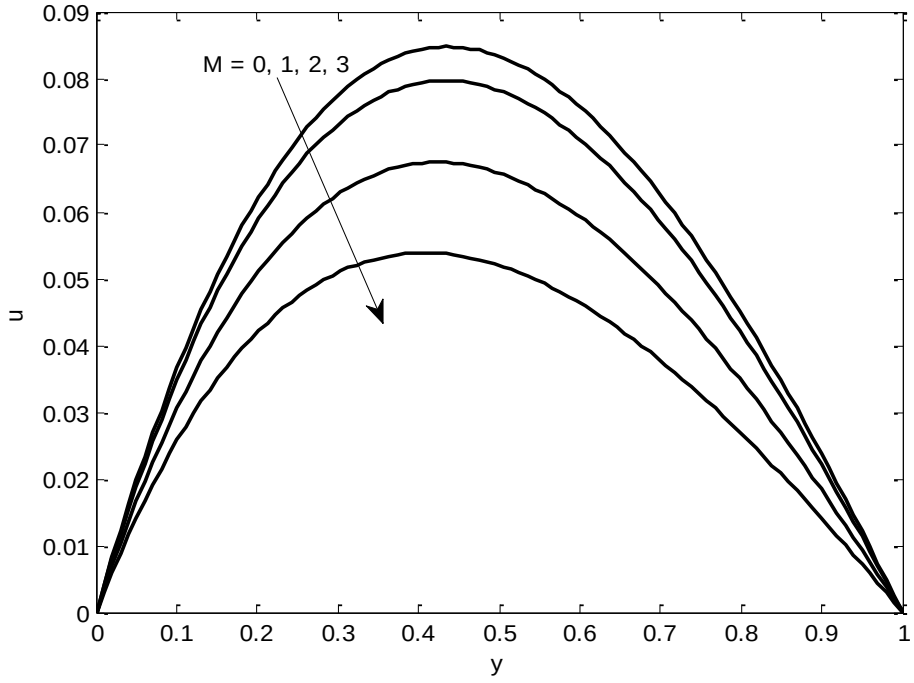

Fig 4: Velocity profiles showing the effects of *M* with $K_p = \lambda = 0$, $R = 0.5, S = 1.0, B = 0.5, K_c = 3.0$ **for** $m = m_1 = 0$.

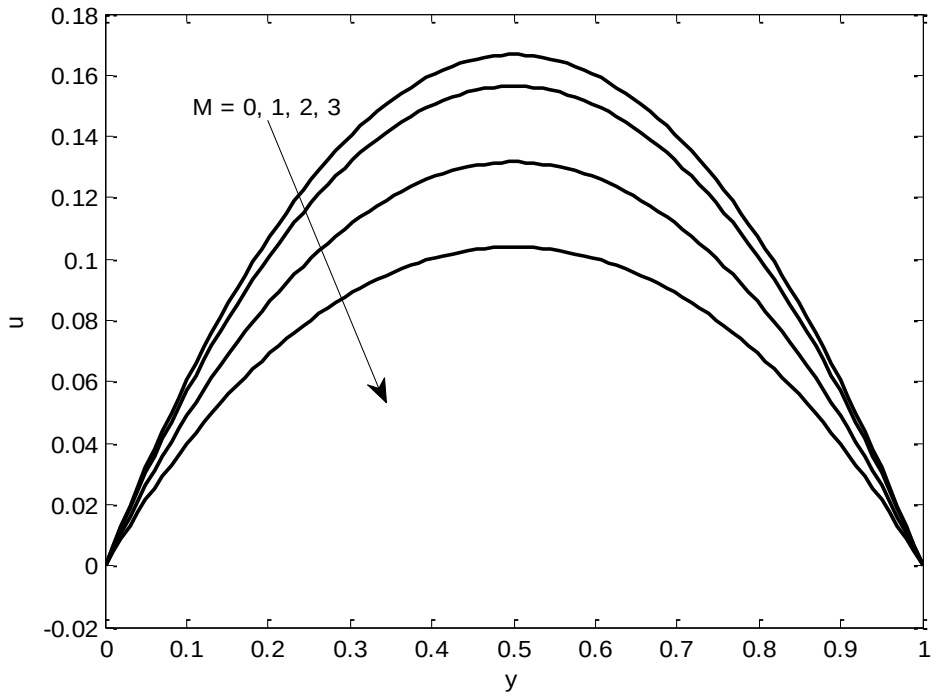

Fig 5: Velocity profiles showing the effects of *M* with, $R = 0.5, S = 1.0, B = 0.5, K_c = 3.0,$ $K_p = \lambda = 0$ **for** $m = m_1 = 1.$

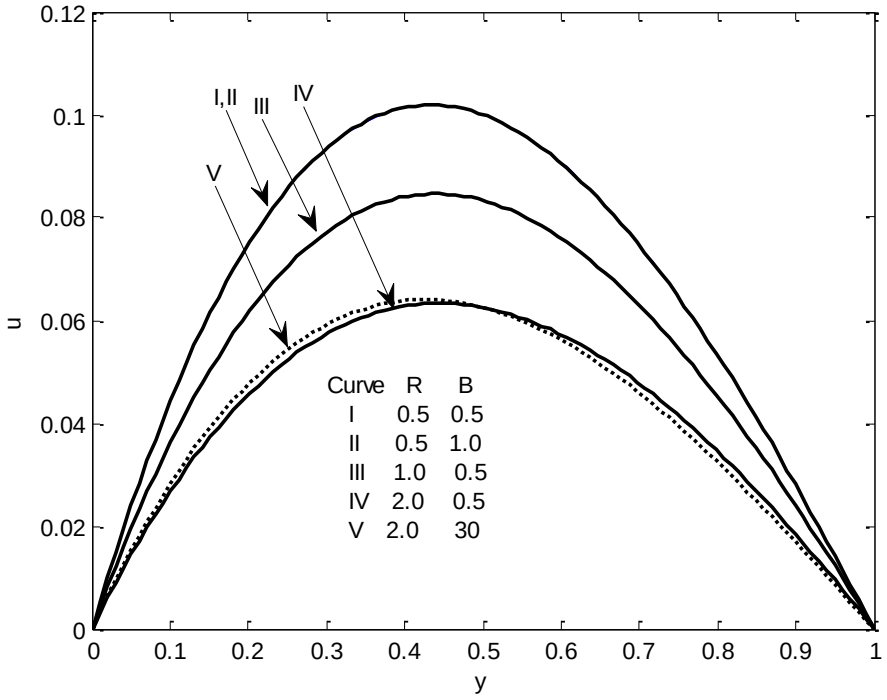

Fig 6: Velocity profiles showing effects of *R* and *B* $(S = 0, K_c = 0)$ **with *M* = 0,** $M = K_p = \lambda = 0$ **for** $m = m_1 = 0$.

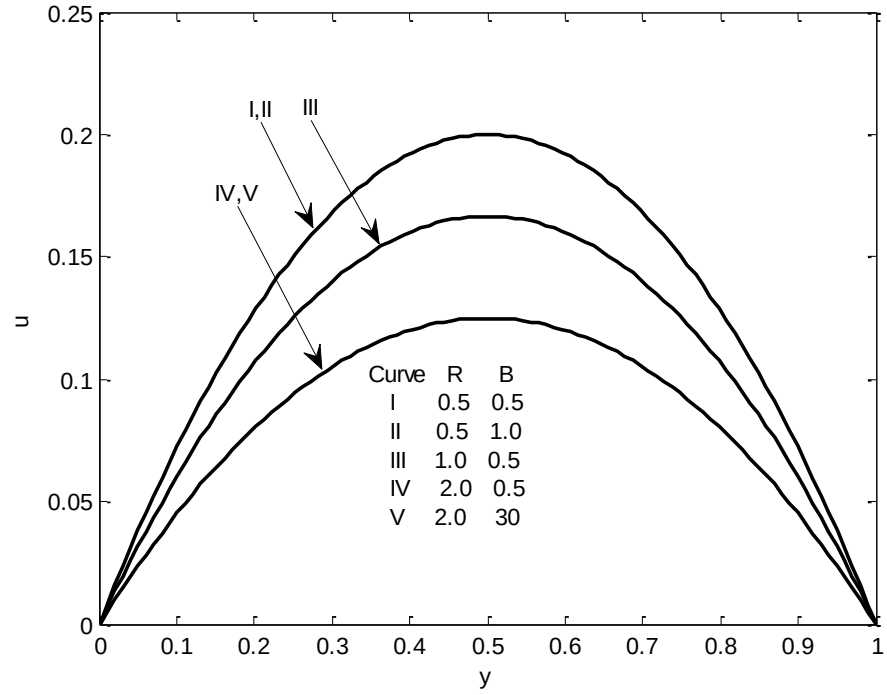

Fig 7 : Velocity profiles showing effects of *R* and *B* $(S = 0, K_c = 0)$ **with** $M = K_p = \lambda = 0$ **for** $m = m_1 = 1$.

The effects of porosity and radiation parameter on the velocity distribution are exhibited in Figs. 8 and 9. It is observed that increase of K_p resists the motion of the flow which in turn reduces the value of velocity in both $m = m_1 = 0$ and $m = m_1 = 1$. This is due to the fact that, the introduction of porous matrix has a tendency to create a drag which in turn offers a resistive force to resist the flow. By this we came to know that boundary layer thickness increases with increase in permeability parameter. It is also observed that the flow velocity is accelerated due to the influence of radiation parameter in both $m = m_1 = 0$ and $m = m_1 = 1$ and thereby increases the boundary layer thickness.

The micro rotation profiles for asymmetric distribution of temperature and concentration in the presence of source/sink and for both types of reactions are shown in Fig. 10. One of the striking features of the variation is that middle layers of the profiles are unaffected due to variation of pertinent parameters governing the flow. This phenomenon is the result of the reverse rotation of the layers beyond the middle of the channel. Another feature is to note that presence of sink under the influence of endothermic reaction causes higher values of $|\omega|$ in the lower half of the channel than that in the presence of source with exothermic reaction. It is also evident that micro-rotation assumes negative values in the lower half where as positive values in the upper half. As regard to the effects of individual parameters, it is clear that an increase in absolute values of heat sink and endothermic reaction, $|\omega|$ increases where as opposite effect is observed in case of material parameter *B*. Further it is concluded that opposite flow behavior is exhibited in the upper half of the channel with respect to material property for $S > 0, K_c > 0$.

The case of symmetric distribution is manifested in Fig. 11. One interesting feature of micro-rotation is that both the categories of profiles ($S > 0, K_c > 0 \& S < 0, K_c < 0$) attain a common point of intersection at middle of the channel whereas in case of asymmetric case it is not the case. Other features of the profile remain same as that of asymmetric case.

The profile on Fig.12 exhibits that an increase in *M* slows down the microrotation (ω) in the layers $y \geq 0.5$ and opposite effect is observed in the other half of the channel in asymmetric case. It is noticed from Fig.13 that the effect of *M* in symmetric case remains same as that of asymmetric case. However, higher microrotation is experienced in the symmetric case.

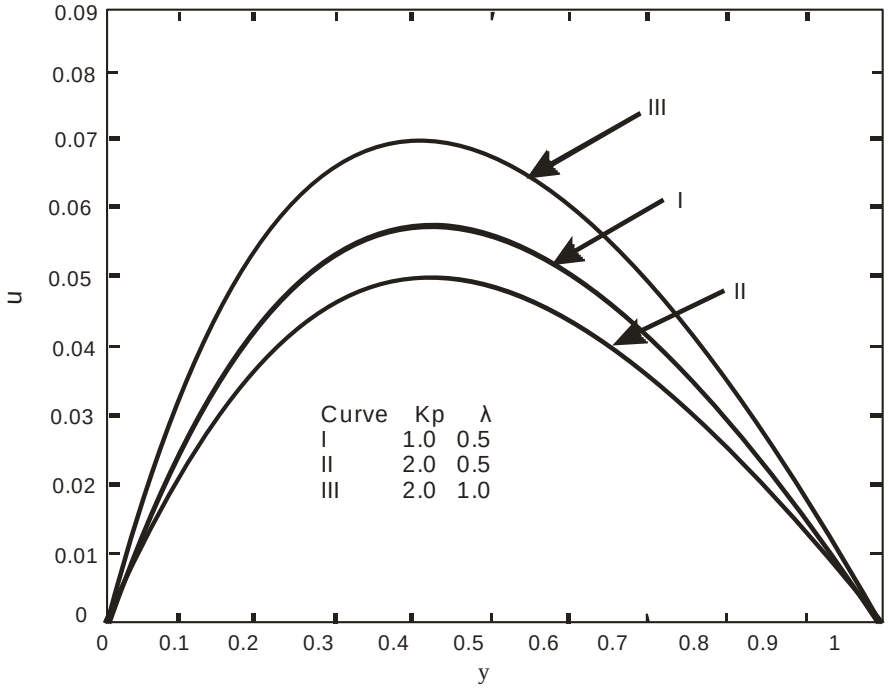

Fig 8: Velocity profiles showing the effect of K_p and λ for R = 0.5, M = 1.0, S = 1.0, B = 0.5, $K_c = 3.0$ and $m = m_1 = 0$.

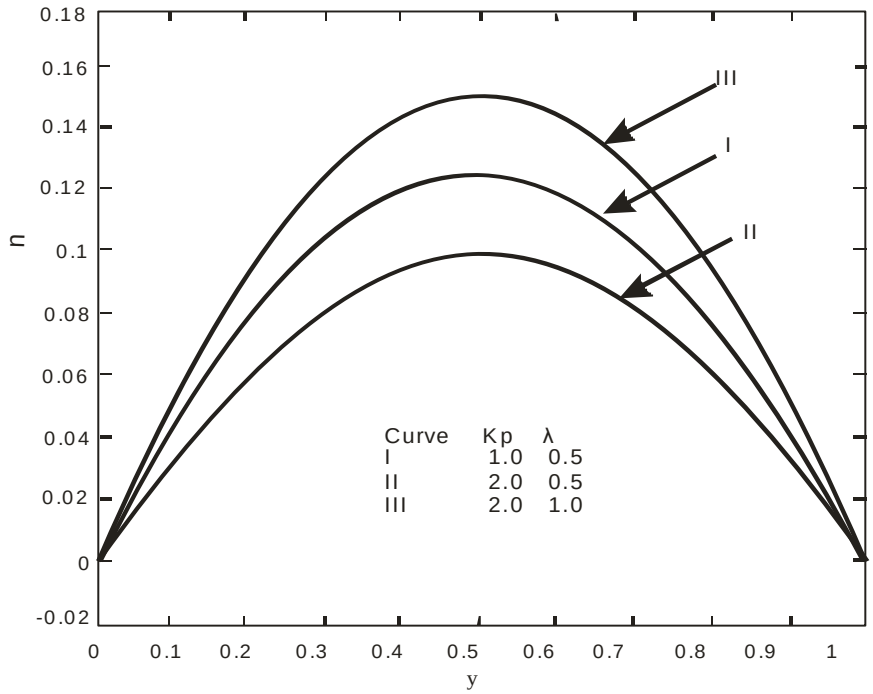

Fig 9: Velocity profiles showing the effect of K_p and λ for R = 0.5, M = 1.0, S = 1.0, B = 0.5, $K_c = 3.0$ and $m = m_1 = 1$.

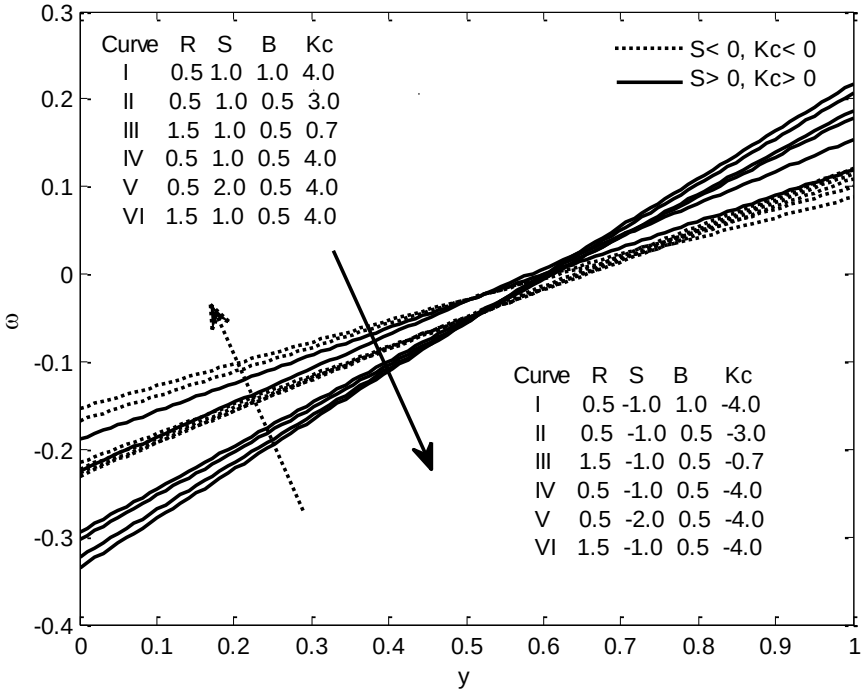

Fig 10. Micro rotation profiles showing the effects of *R, S, B,* K_c with $M = K_p = \lambda = 0$ for $m = m_1 = 0$.

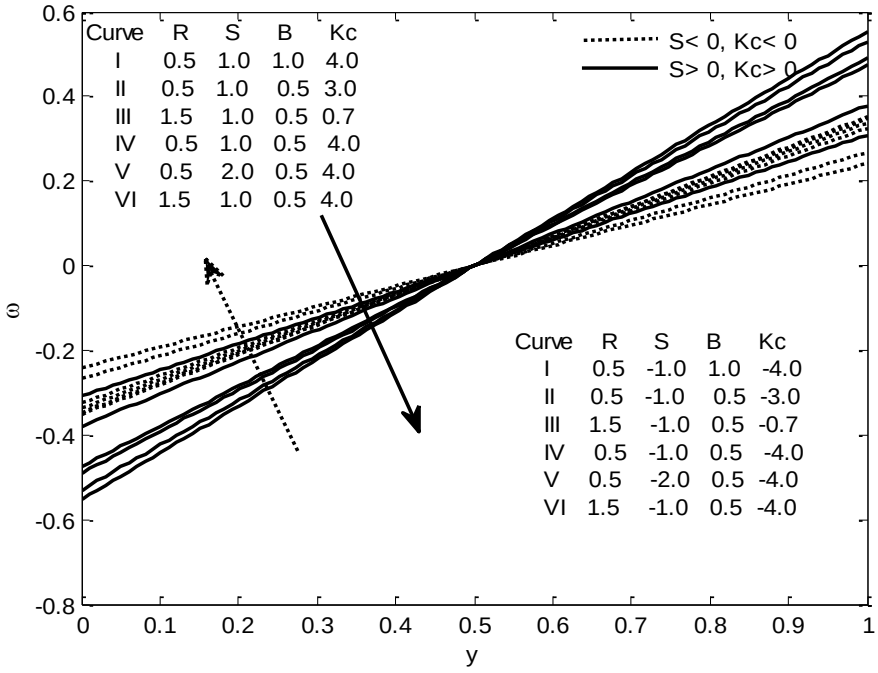

Fig 11: Micro rotation profiles showing the effects of *R, S, B,* K_c with $M = K_p = \lambda = 0$ for $m = m_1 = 1$.

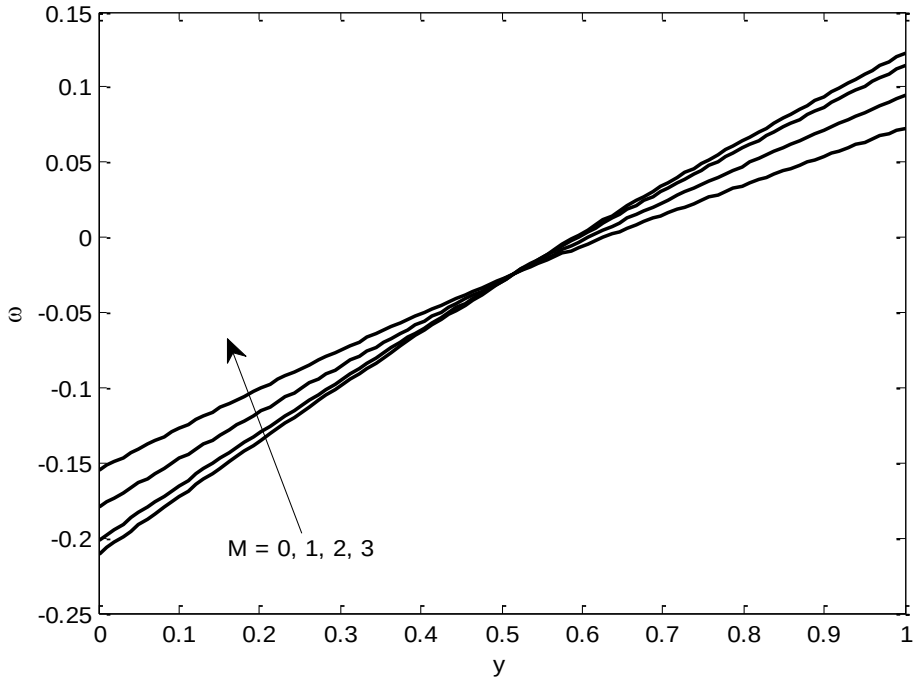

Fig 12 : Microrotation profiles showing the effects of *M* with $R = 0.5, S = 1.0, B = 0.5, K_c = 3.0, K_p = \lambda = 0$ **for** $m = m_1 = 0$.

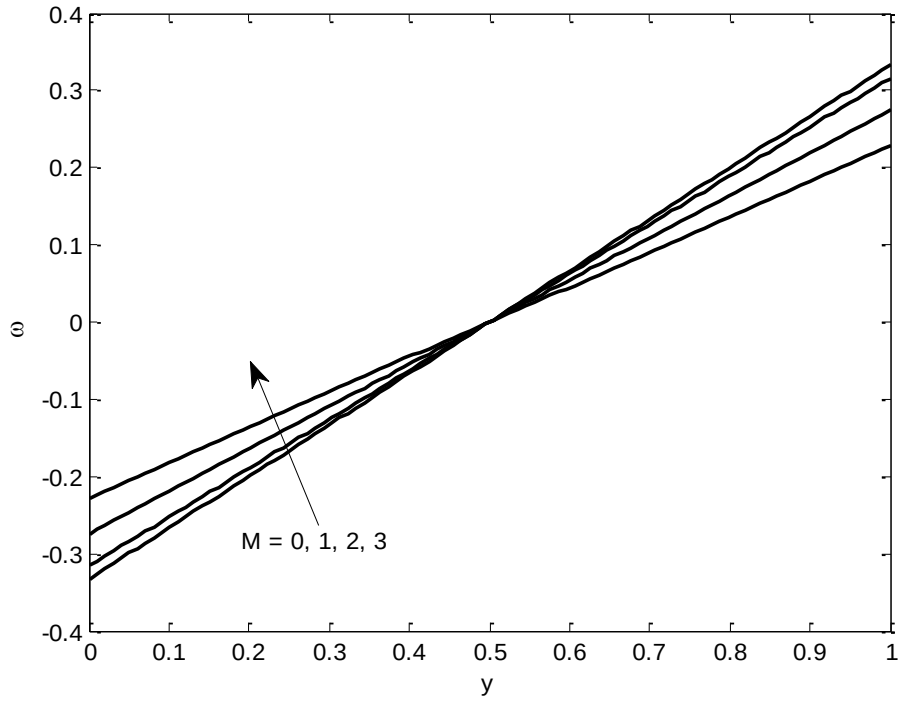

Fig 13 : Microrotation profiles showing the effects of *M* with $R = 0.5, S = 1.0, B = 0.5, K_c = 3.0, K_p = \lambda = 0$ **for** $m = m_1 = 1$.

One important observation from Figs. 14 and 15 is that the effect of material property of micropolar fluid on microrotation is not prominent in the absence of source and chemical reaction which is evident from the curves IV and V. It is also observed that an increase in vortex viscosity parameter decelerates $|\omega|$ while other features remaining same.

The influences of porous matrix on the micro rotation in both symmetric and asymmetric cases are manifested in Figs. 16 and 17. It is remarked that an increase in permeability parameter decreases the microrotation (ω) in the layers $y \geq 0.5$ and the opposite effect is observed in the other half of the channel in asymmetric case. However, the effect of K_p in the symmetric case remains the same as that of the asymmetric case. Aboveall, higher micro rotation is achieved in the symmetric case. The effect of radiation parameter (λ) causes an enhancement of micro rotation in the first half of the porous channel whereas the opposite effect is produced in the second half of the channel. However, higher mocro rotation is developed due to the influence of R for $m = m_1 = 0$.

The nature of temperature profiles in the presence of thermal radiation for two values of temperature (m = 0 and 1) is illustrated in Fig. 18. It is reveals that temperature gets enhanced at all points due to increase in λ. It is interesting to note that the distribution is almost symmetric and parabolic for $m = 1$ whereas a sharp fall is noticed for $m = 0$ irrespective the value of λ. The increase in temperature gradient due to increase in λ leads to thinning of thermal boundary layer.

A graphical representation of temperature variation for source or sink and two values of temperature ($m = 0$ and 1) is shown in Fig. 19. Eqn. (10) is a linear equation and the corresponding boundary conditions signify that temperature variation is controlled by source and temperature parameter. Fig.19 also provides enhanced temperature distribution at all points when S varies from -1 to 3. In the present case when $m = 1$, the distribution is almost symmetrical and parabolic but when $m = 0$, the sharp fall of temperature is well marked. Since the temperature at the lower plate is fixed at 1.0, the temperature at the upper plate matters for generating thermal gradient and hence the thinning/thickening of thermal boundary layer.

The variation of concentration is exactly similar to that of temperature as the source/ sink is replaced by exothermic/endothermic reaction of first order as shown in Fig. 20.

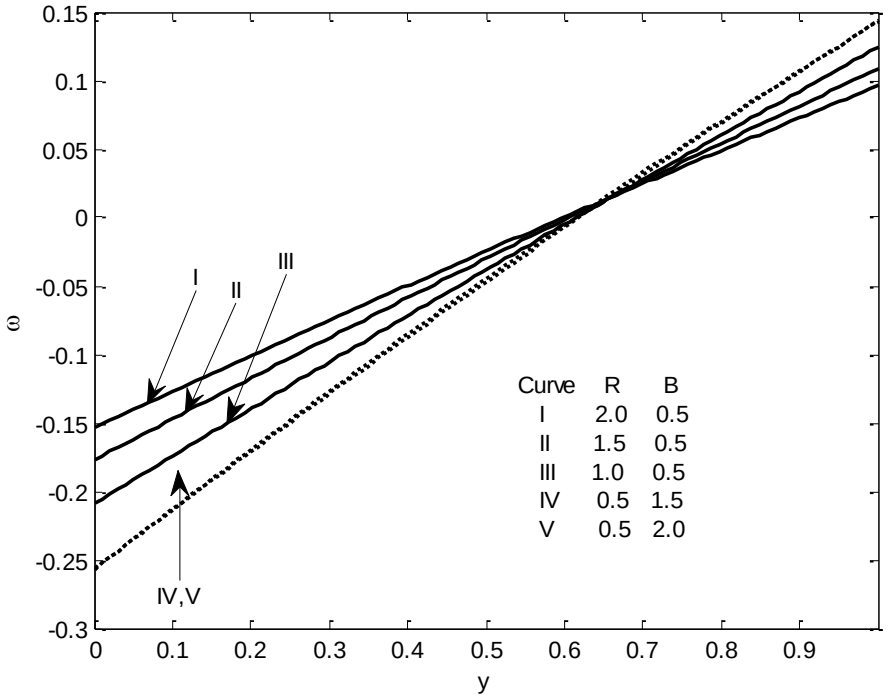

Fig 14 : Micro rotation profiles showing the effects of *R* and *B* $(S=0, K_c=0)$ **with** $M=K_p=\lambda=0$ **for** $m=m_1=0$.

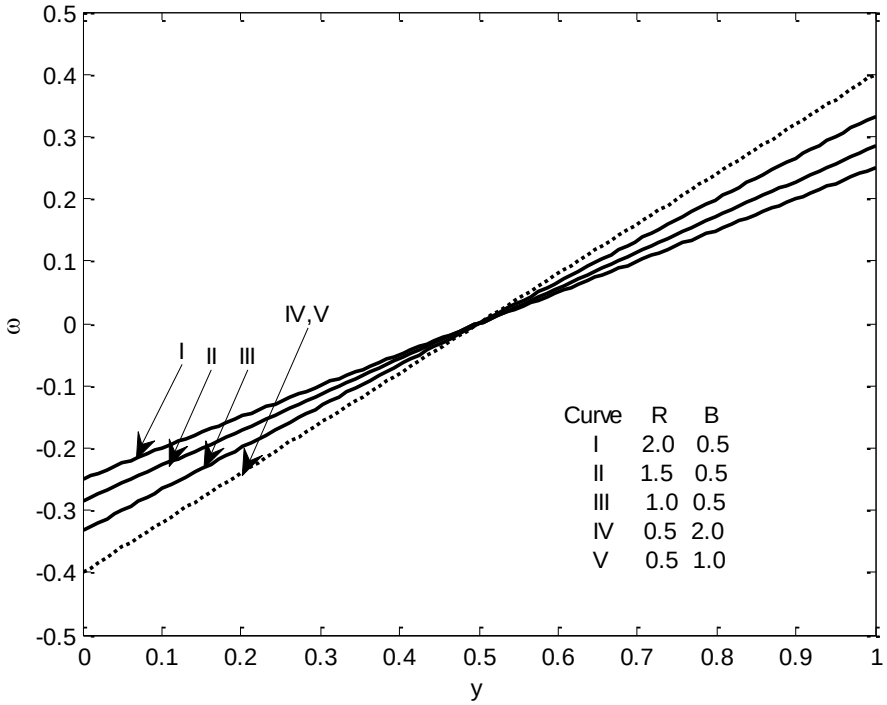

Fig 15 : Micro rotation profiles showing the effects of *R* and *B* $(S=0, K_c=0)$ **with** $M=K_p=\lambda=0$ **for** $m=m_1=1$.

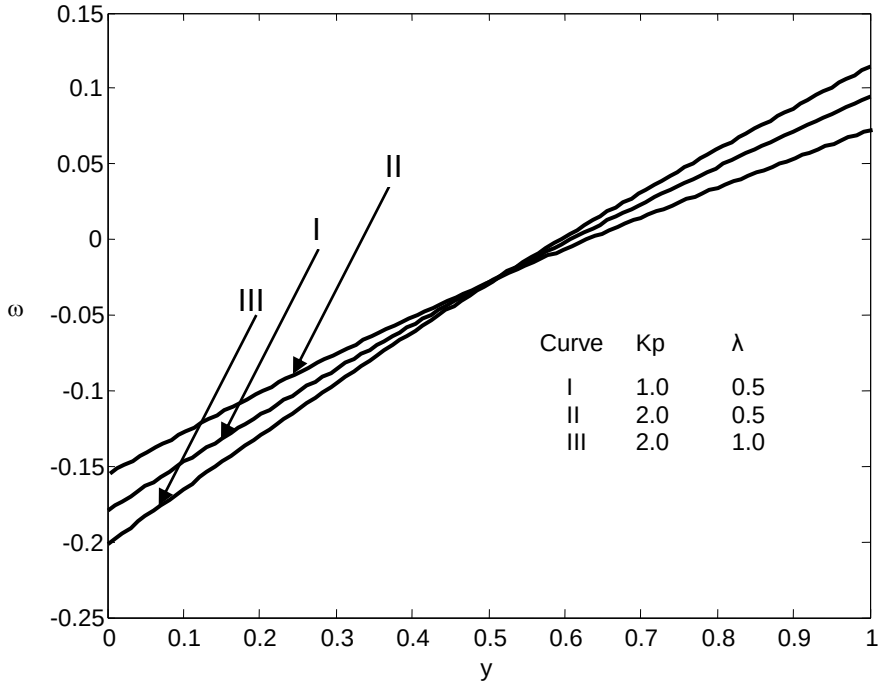

Fig 16 : Microrotation profiles showing the effect of K_p and λ for R = 0.5, S = 1.0, B = 0.5, $K_c = 3.0$ and $m = m_1 = 0$.

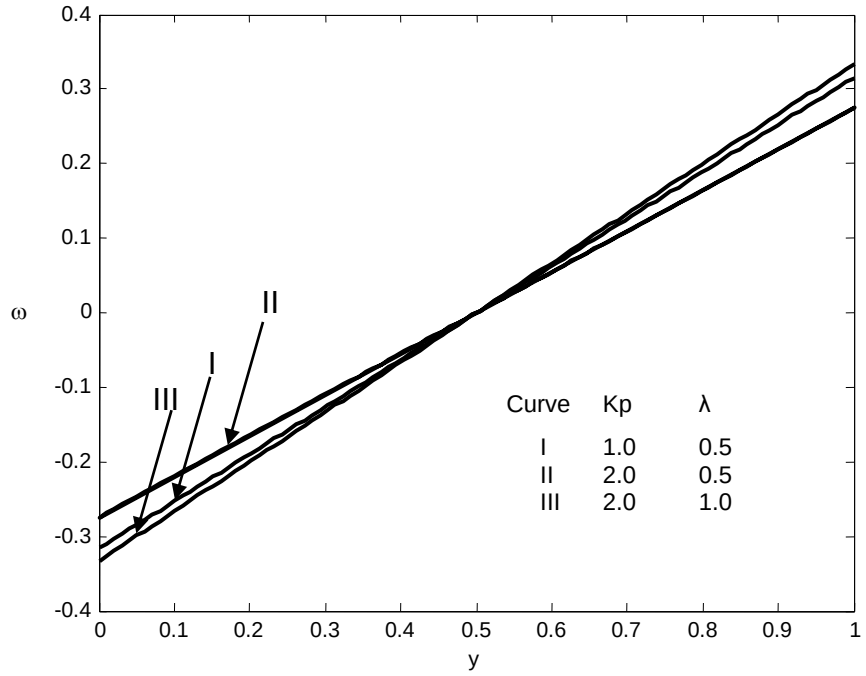

Fig 17 : Microrotation profiles showing the effect of K_p and λ for R = 0.5, S = 1.0, B = 0.5, $K_c = 3.0$ and $m = m_1 = 1$.

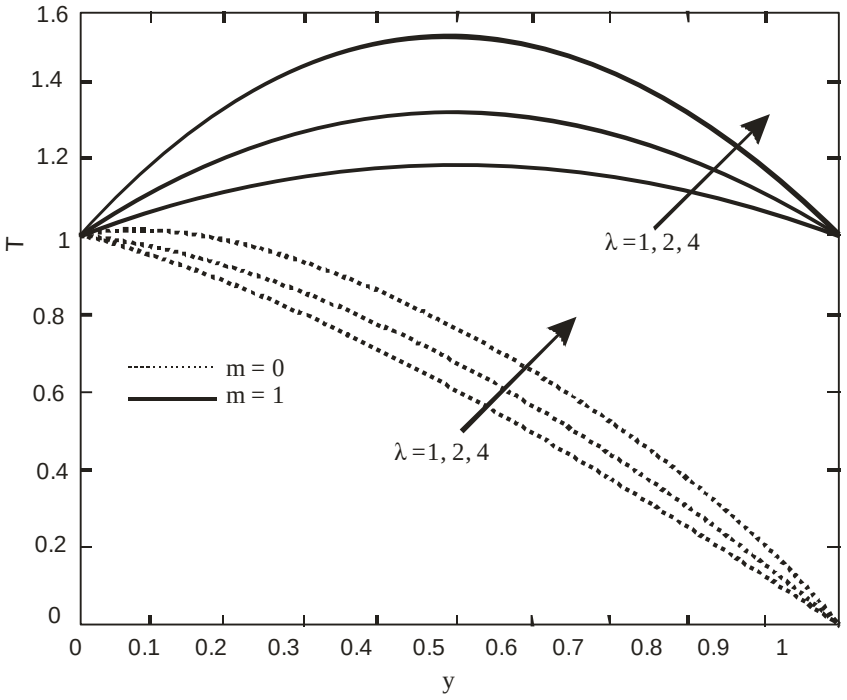

Fig 18 : Temperature profiles for different values of λ for $m=0$ and $m=1$.

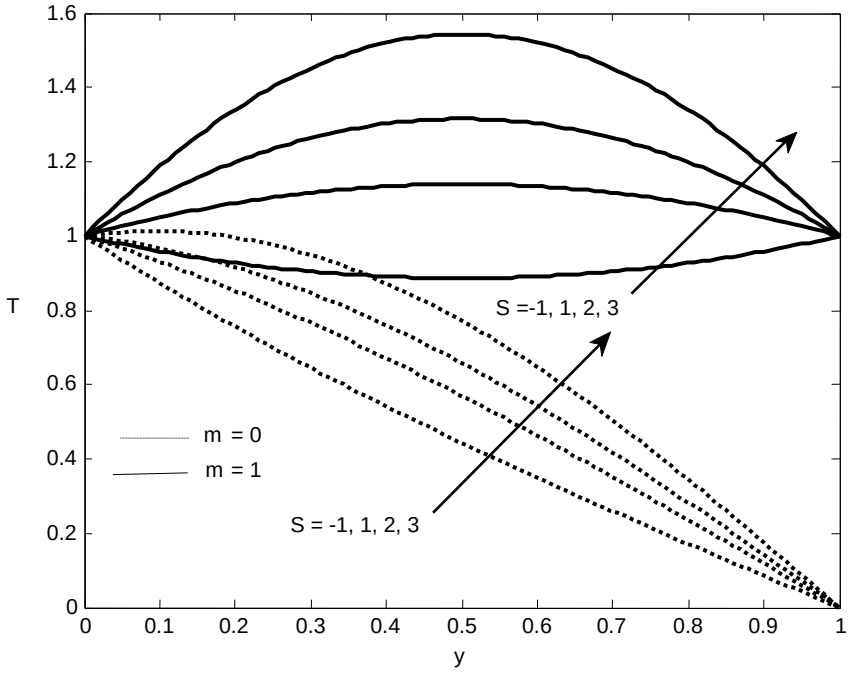

Fig 19: Temperature profiles for different values of *S* for $m=0$ **and** $m=1$.

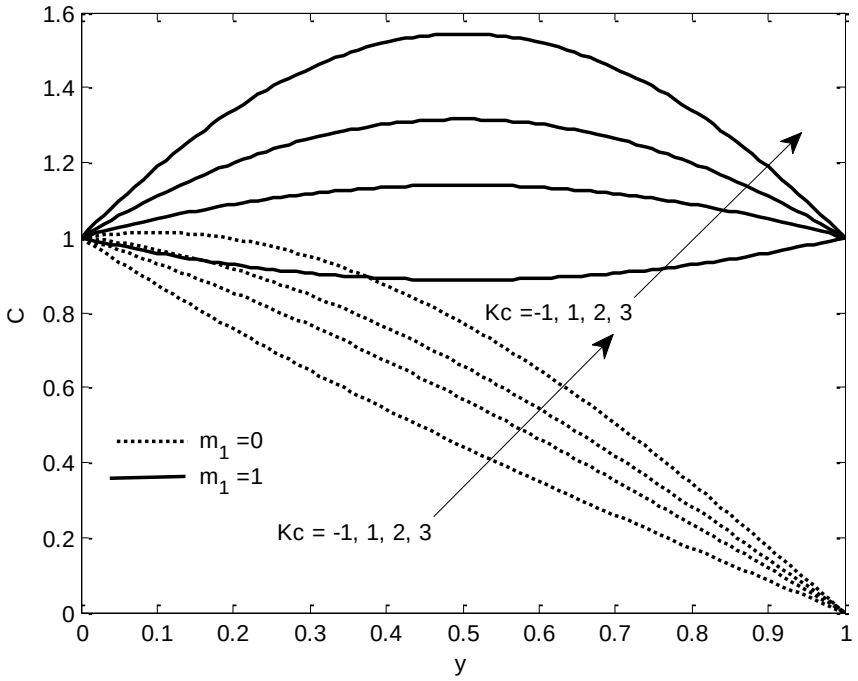

Fig 20: Concentration profiles for different values of *S* for $m_1 = 0$ and $m_1 = 1$.

Table 1 enlists the maximum values of u in asymmetric case ($m = m_1 = 0$). The velocity attains maximum increase from 0.09967 to 0.16187 by 38.43% for $S > 0, K_c > 0$ while it increases from 0.05934 to 0.09401 by 36.88% for $S < 0, K_c < 0$. Table 2 shows variation of u_{max} with respect to variation of R, S, B, K_c for $S > 0, K_c > 0$ and $S < 0, K_c < 0$ in asymmetric case. Table 2 shows the variation of u_{max} with respect to variation of *R*, *S*, *B*, K_c for $S > 0, K_c > 0$ and $S < 0, K_c < 0$ in asymmetric case ($m = m_1 = 0$).

Table 3 enlists the maximum values of u in symmetric case ($m = m_1 = 1$).The velocity attains maximum increase from 0.19769 to 0.29302 by 32.53% at $y = 0.5$ for $S > 0, K_c > 0$ and 0.12055 to 0.17075 by 29.4% at $y = 0.5$ for $S < 0, K_c < 0$. Table 4 shows the variation of u_{max} with respect to variation of R, S, B, K_c for S > 0, K_c > 0 and S < 0, K_c< 0 in symmetric case.

Table 4 shows the variation of u_{max} with respect to variation of *R*, *S*, *B*, K_c for S > 0, K_c > 0 and S < 0, K_c< 0 in symmetric case.

Table 1: The magnitude of u_{max} with respect to *y* for $S>0, K_c>0$ and $S<0, K_c<0$ in asymmetric case.

Source & Exothermic; Sink & Endothermic	Distance (y)	u_{max}	Graphical representation	Maximum increase of u_{max} (%)
Source & Exothermic ($S>0, K_c>0$)	0.46	0.09967	Curve V	38.43
	0.45	0.11118	Curve VI	
	0.44	0.12413	Curve III	
	0.44	0.12895	Curve I	
	0.45	0.14099	Curve II	
	0.46	0.16187	Curve IV	
Sink & Endothermic ($S<0, K_c<0$)	0.45	0.05934	Curve V	36.88
	0.44	0.07935	Curve IV	
	0.43	0.08317	Curve II	
	0.43	0.08589	Curve I	
	0.44	0.08741	Curve III	
	0.45	0.09401	Curve VI	

Table 2 : Variation of u_{max} with respect to variation of R, S, B, K_c for $S>0, K_c>0$ and $S<0, K_c<0$ in asymmetric case.

Source & Exothermic; Sink & Endothermic	Physical parameters	Graphical representation	u_{max}
Source & Exothermic ($S>0$, $K_c>0$)	$0.5 \le R \le 1.5$	Curve II & Curve V	$0.09967 \le u_{max} \le 0.14099$
	$1.0 \le S \le 2.0$	Curve II & Curve IV	$0.14099 \le u_{max} \le 0.16187$
	$0.5 \le B \le 1.0$	Curve II & Curve III	$0.12413 \le u_{max} \le 0.14099$
	$0.7 \le K_c \le 3.0$	Curve VI & Curve I	$0.11118 \le u_{max} \le 0.12895$
Sink & Endothermic ($S<0$, $K_c<0$)	$0.5 \le R \le 1.5$	Curve II & Curve V	$0.05934 \le u_{max} \le 0.08317$
	$-2.0 \le S \le -1.0$	Curve IV & Curve II	$0.07935 \le u_{max} \le 0.08317$
	$0.5 \le B \le 1.0$	Curve II & Curve III	$0.08317 \le u_{max} \le 0.08741$
	$-3.0 \le K_c \le -0.7$	Curve VI & Curve I	$0.08589 \le u_{max} \le 0.0901$

Table 3: The magnitude of u_{max} with respect to *y* for S > 0, K_c > 0 and S< 0, K_c< 0 in symmetric case.

Source & Exothermic; Sink & Endothermic	Distance (y)	u_{max}	Graphical representation	Maximum increase of u_{max} (%)
Source & Exothermic $(S>0, K_c>0)$	y = 0.5	0.19769	Curve V	32.53
		0.21878	Curve VI	
		0.24493	Curve III	
		0.25461	Curve I	
		0.27896	Curve II	
		0.29302	Curve IV	
Sink & Endothermic $(S<0, K_c<0)$		0.12055	Curve V	29.4
		0.15458	Curve IV	
		0.16218	Curve II	
		0.16767	Curve I	
		0.16978	Curve III	
		0.17075	Curve VI	

Table 4: Variation of u_{max} with respect to variation of R, S, B, K_c for S > 0, K_c > 0 and S < 0, K_c< 0 in symmetric case.

Source & Exothermic; Sink & Endothermic	Physical parameters	Graphical representation	u_{max}
Source & Exothermic $(S>0, K_c>0)$	$0.5 \le R \le 1.5$	Curve II & Curve V	$0.19769 \le u_{\max} \le 0.27896$
	$1.0 \le S \le 2.0$	Curve II & Curve IV	$0.27896 \le u_{\max} \le 0.29302$
	$0.5 \le B \le 1.0$	Curve II & Curve III	$0.24493 \le u_{\max} \le 0.27896$
	$0.7 \le K_c \le 3.0$	Curve VI & Curve I	$0.21878 \le u_{\max} \le 0.25461$
Sink & Endothermic $(S<0, K_c<0)$	$0.5 \le R \le 1.5$	Curve II & Curve V	$0.11655 \le u_{\max} \le 0.16218$
	$-2.0 \le S \le -1.0$	Curve IV & Curve II	$0.15458 \le u_{\max} \le 0.16218$
	$0.5 \le B \le 1.0$	Curve II & Curve III	$0.16218 \le u_{\max} \le 0.17075$
	$-3.0 \le K_c \le -0.7$	Curve VI & Curve I	$0.16767 \le u_{\max} \le 0.17075$

Conclusion

The major findings from the present study can be summarized as follows:

- Presence of heat source and exothermic reaction enhances the velocity at all points overriding the effects of vortex viscosity and material property in both symmetric and asymmetric cases.
- Vortex viscosity parameter has dominating effect attributing micropolar properties.
- Vortex viscosity has a retarding effect on fluid velocity.
- Micro-rotation remains unaffected by the controlling parameters of the flow phenomena in the middle layers of the channels as the middle layers experience two mutual opposite rotations.
- The resistive force of electromagnetic origin (Lorentz force) produced by the interaction of the current and applied magnetic field due to conducting micropolar fluid resists the velocity at all points of the channel and also resists the microrotation in the right half of the channel with an increasing magnetic parameter (M).
- The porous matrix opposes the velocity at all points of the channel and also opposes the microrotation in the right half of the channel.
- The increase in temperature gradient due to increase in radiation parameter (λ) leads to thinning of thermal boundary layer.

References

[1] A.C. Eringen, Theory of micropolar fluids, J. Math. Mech., 16, 1–18, 1966.

[2] M. K. Nayak, Industrial micropolar fluids: Synthesis and Applications, 2nd ed., India Tech, New Delhi, 2014.

[3] M.M. Rahman, I.A. Eltayeb, S.M. Mujibur Rahman, Thermo-micropolar fluid flow along a vertical permeable plate with uniform surface heat flux in the presence of heat generation, Therm. Sci., 13, (1), 23–36, 2009.

[4] M.M. Rahman, Convective flows of micropolar fluids from radiative isothermal porous surfaces with viscous dissipation and joule heating, Commn. Nonlinear Sci. Numer. Simulat., 14, (7), 3018–3030, 2009.

[5] M.M. Rahman, T. Sultana, Radiative heat transfer flow of micropolar fluid with variable heat flux in a porous medium, Nonlinear Anal.: Model. Control 13, (1), 71–87, 2008.

[6] M.M. Rahman, T. Sultana, Transient convective flow of micropolar fluid past a continuously moving vertical porous plate in the presence of radiation, Int. J. Appl. Mech. Eng., 12, (2), 497–513, 2007.

[7] M.M. Rahman, M.A. Sattar, MHD convective flow of a micropolar fluid past a continuously moving vertical porous plate in the presence of heat generation/absorption, ASME J. Heat Trans., 128, (2), 142–152, 2006.

[8] O. Abdulaziz, I. Hashim, Fully developed free convection heat and mass transfer of a micropolar fluid between porous vertical plates, Numer. Heat Transfer, Part A: Applications, 55, (3), 270–288, 2009.

[9] H.A.M. El-Arabawy, Effect of suction/injection on the flow of a micropolar fluid past a continuously moving plate in the presence of radiation, Int. J. Heat Mass Transfer, 46, 1471–1477, 2003.

[10] M. K. Nayak, G. C. Dash, L. P. Singh, Unsteady radiative MHD free convective flow and mass transfer of a viscoelastic fluid past an inclined porous plate, Arab. J. Sci. Eng., 40, 3029-3039, 2015.

[11] A. J. Chamkha, T. Grosan, I. Pop, Fully developed free convection of a micropolar fluid in a vertical channel, Int. Comm. Heat Transfer, 29, 1021–1196, 2002.

[12] S. K. Parida, M. Acharya, G.C. Dash, S. Panda, MHD heat and mass transfer in a rotating system with periodic suction, Arab. J. Sci. Eng., 36, (6), 1139-1151, 2011.

[13] J. Zueco, S. Ahmed, L. M. López-Ochoa, Magneto-micropolar flow over a stretching surface embedded in a Darcian porous medium by the numerical network method, Arab. J. Sci. Eng., 39, (6), 5141-5151, 2014.

[14] N.T. Eldabe, Mohamed Y. Abou-zeid, Magnetohydrodynamic peristaltic flow with heat and mass transfer of micropolar biviscosity fluid through a porous medium between two co-axial tubes, Arab. J. Sci. Eng., 39, (6), 5045-5062, 2014.

[15] M. Kar, S. N. Sahoo, P. K. Rath, G. C. Dash, Heat and mass transfer effects on a dissipative and radiative visco-elastic MHD flow over a stretching porous sheet, Arab. J. Sci. Eng., 39, (5), 3393-3401, 2014.

[16] K. A. Helmy, H. F. Idriss, S. E. Kassem, MHD free convection flow of a micropolar fluid past a vertical porous plate, Canadian J. of Phys., 80, (12), 1661–1673, 2002.

[17] M. K. Nayak, G. C. Dash, L. P. Singh, Effect of chemical reaction on MHD flow of a viscoelastic fluid through porous medium, JAAC, 4, (4), 367-381, 2014.

[18] B. Mohanty, S.R. Mishra, H.B. Pattanayak, Numerical investigation on heat and mass transfer effect of micropolar fluid over a stretching sheet through porous media, Alexandria Eng. Journal, 54, 223–232, 2015.

[19] D. B. Ingham, I Pop, Transport phenomena in Porous Media, Elsevier Sc. Ltd., U. K., 1998.

[20] K. Vafai, Handbook of Porous Media, 2nd ed., Taylor and Francis, New York, 2005.

[21] M. K. Nayak, Flow through porous media, 1st ed., India Tech, New Delhi, 2015.

[22] A. Bejan, Convection Heat Transfer, 4th ed., Wiley, New York, 2013.

[23] I. A. Nield, A. Bejan, Convection in Porous Media, 4th ed., Springer, New York, 2012.

[24] F. P. Foraboschi, I. Di Federico, Heat transfer in laminar flow of non-Newtonian heat-generating fluids, Int. J. Heat Mass Transfer, 7, (3), 315-318, 1964.

[25] M. J. Babu, R. Gupta, N. Sandeep, Effect of radiation and viscous dissipation on stagnation-point flow of a micropolar fluid over a nonlinearly stretching surface with suction/injection, J. Basic Appl. Research Int., 7, (2), 73-82, 2015.

[26] R. Muthucumaraswamy, Effects of a chemical reaction on a moving isothermal vertical surface with suction, Acta Mechanica, 155, (1), 65-70, 2002.

[27] M. K. Nayak, G. C. Dash, L. P. Singh, Steady free convection and mass transfer MHD flow of a micropolar fluid in a vertical channel with heat source and chemical reaction, Walailak J Sci & Tech, 12, (9), 785-804, 2015.

[28] K. R. Cramer, Shih-I Pai, Magnetofluid dynamics for Engineers and applied Physics, Script publishing company, Washington D.C., pg 144, 1973.

[29] Shih-I Pai, Viscous flow theory, D. Van Nostrand Company, Inc. pg 223, 1956.

[30] M. Q. Brewster, Thermal radiative transfer properties, Wiley, New York, 1972.

[31] M. Khan, E. Sanjayan, Viscoelastic boundary layer flow and heat transfer over an exponential stretching sheet, Int. J. Heat Mass Transfer, 48, 1534-1542, 2005.